

OAML: Outlier Aware Metric Learning for OOD Detection Enhancement

Heng Gao^{1*}, Zhuolin He^{2*}, Shoumeng Qiu², and Jian Pu^{1†}

¹ Institute of Science and Technology for Brain-Inspired Intelligence, Fudan University

² School of Computer Science, Fudan University

{hgao22,zlhe22}@m.fudan.edu.cn, skyshoumeng@163.com, jianpu@fudan.edu.cn

<https://github.com/HengGao12/OAML>

Abstract. Out-of-distribution (OOD) detection methods have been developed to identify objects that a model has not seen during training. The Outlier Exposure (OE) methods use auxiliary datasets to train OOD detectors directly. However, the collection and learning of representative OOD samples may pose challenges. To tackle these issues, we propose the Outlier Aware Metric Learning (OAML) framework. The main idea of our method is to use the k-NN algorithm and Stable Diffusion model to generate outliers for training at the feature level without making any distributional assumptions. To increase feature discrepancies in the semantic space, we develop a mutual information-based contrastive learning approach for learning from OOD data effectively. Both theoretical and empirical results confirm the effectiveness of this contrastive learning technique. Furthermore, we incorporate knowledge distillation into our learning framework to prevent degradation of in-distribution classification accuracy. The combination of contrastive learning and knowledge distillation algorithms significantly enhances the performance of OOD detection. Experimental results across various datasets show that our method significantly outperforms previous OE methods.

Keywords: Machine Learning Safety, Out-of-Distribution Detection, Outlier Exposure Training, Metric Learning, Outlier Data Synthesis.

1 Introduction

To prevent machine learning models from delivering unreliable predictions when encountering inputs that deviate from their training data distribution, many Out-of-Distribution (OOD) detection algorithms have been proposed. These methods enable models to discern In-Distribution (ID) and OOD samples during the inference phase, thereby paving the way for trustworthy AI systems. Generally, these approaches can be categorized into three main types: Post-hoc methods [14, 18, 22, 23], Outlier Exposure (OE) methods [11, 17, 43], and Representation Learning-based methods [26, 31, 40].

*Equal contribution.

†Corresponding author.

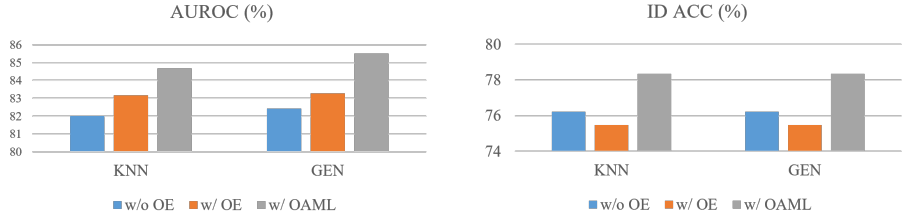


Fig. 1: In this figure, we compare the AUROC (left) and ID accuracy (right) across three training settings: vanilla training, training with basic outlier exposure [17], and training with OAML (ours) using KNN [33] and GEN [24] as the score functions.

Outlier Exposure methods utilize a set of auxiliary OOD samples to enhance the model’s ability to detect OOD instances. The main challenges for these methods are: (i) collecting representative OOD samples, and (ii) effectively learning from a combination of ID and OOD data. In recent work, Du et al. [9] propose DreamOOD, which leverages Stable Diffusion (SD) [29] to generate OOD samples in pixel space. However, synthesizing images in the high dimensional pixel space can be difficult to optimize [42], which is empirically shown in VOS [11]. Furthermore, as demonstrated by our experiments in Figure 1, we observed that the ID accuracy decreases after introducing collected pixel-level OOD samples for training. But according to the definition in Yang et al.’s work [42], **OOD detection should not harm the ID classification accuracy.**

Motivated by these observations, we develop an Outlier Aware Metric Learning (OAML) framework that collects and trains with outliers *in the latent space*. Specifically, we use the k-Nearest Neighbour (k-NN) [19] algorithm to sample outliers from the latent space of transformer encoders. These outliers are then used as token conditions for Stable Diffusion to generate OOD features for outlier exposure training. Subsequently, we design a mutual information-based feature contrastive learning approach to enlarge discrepancies between ID and OOD data distribution at the feature level. We verify the effectiveness of this contrastive learning method both empirically and theoretically. Moreover, we introduce knowledge distillation into our learning framework to leverage the "dark knowledge" from the teacher model for preventing the degradation of ID accuracy when training with mixed ID and OOD data. To our surprise, it has improvements in both ID and OOD detection performance. The experiments conducted with our framework on CIFAR-10/100 [20] and ImageNet-1k [5] achieve non-trivial benefits for OOD detection performance.

In a nutshell, our main contributions can be summarized as follows:

- We propose the Outlier Aware Metric Learning (OAML) framework, which generates OOD data in the latent space using Stable Diffusion to facilitate network optimization during training with outliers.

- We develop a mutual information-based feature contrastive learning method to enlarge the feature discrepancy between ID and OOD data, aided by knowledge distillation from a large teacher model, thereby preventing the degradation of ID performance and further enhancing OOD detection results.
- We empirically illustrate significant improvements in several metrics (FPR95, AUROC) using different kinds of score functions on both CIFAR-10/100 [20] and ImageNet-1k [5] benchmarks.

2 Related Work

Outlier Exposure-based OOD Detection. The key to outlier exposure-based approaches is to train by collecting OOD samples, improving the model’s ability to discern between ID and OOD data. Hendrycks et al. [17] propose to utilize an auxiliary dataset as the outlier data for training the OOD detector, thereby enhancing its OOD detection performance. In VOS [11], Du et al. propose to sample OOD data from a class-conditional distribution in the feature space for regularizing the decision boundary between ID and OOD data. Similar to VOS, Tao et al. [35] also propose to sample outliers in the latent space. They do not make any distributional assumptions on the ID embeddings. Recently, Du et al. proposed DreamOOD [9], which is an outlier synthesis method based on Stable Diffusion [29], which generates OOD samples in the pixel space. Different from NPOS [35] and DreamOOD [9], we do not sample outliers in the CLIP [28] latent space but in the original image space of the large teacher model. Because the conditional control may constrain the diversity of the OOD samples, which will limit the OOD information that can be learned during training.

Representation Learning-based OOD Detection. The motivation for the representation learning-based method is to improve the quality of features, thereby enhancing the performance of OOD detection. Sehwag et al. [31] and Winkens et al. [40] have empirically demonstrated the effectiveness of representation learning techniques in OOD detection by applying contrast learning methods. Jihoon et al. [34] propose CSI, a method that enhances the SimCLR [2] framework by incorporating OOD features into an image transformation technique, thereby expanding the contrast learning model’s ability to distinguish a wider range of negative examples. This approach utilizes a composite score function that amalgamates scores derived from features trained via contrast learning to distinguish both ID and OOD samples. Du et al. [8] introduced SIREN, which innovatively embeds features onto a unit sphere following a mixed von Mises-Fisher distribution, facilitated by a trainable loss function. In our research, we explore the untapped potential of knowledge distillation in the context of OOD detection, verifying its effectiveness in preventing ID accuracy degradation.

3 Preliminaries

OOD Detection. For a machine learning model to be effectively deployed in the real world, it must reliably identify ID samples and accurately recognize

OOD samples. Formally, given a test sample \mathbf{x} and a pre-trained classifier $f(\cdot)$, an OOD detection decision function can be written as

$$\mathcal{G}_\lambda(\mathbf{x}) = \begin{cases} \text{ID}, & S(\mathbf{x}) \geq \alpha, \\ \text{OOD}, & S(\mathbf{x}) < \alpha, \end{cases}$$

where α is the threshold, ID means that sample \mathbf{x} comes from the in-distribution dataset and OOD means that the sample \mathbf{x} comes from the out-of-distribution dataset.

Proper Scoring Rules. Let $\mathbf{x} \in \mathcal{X}$ be a test sample seen by the model in the inference phase. Denote p as the probability prediction output of classifier $f(\mathbf{x}) = h(g(\mathbf{x}))$, where $h(\cdot)$ is the classification head, and $g(\cdot)$ is the feature extractor that outputs the feature map of the penultimate layer.

The scoring rules are mostly real-valued functions. Tilmann et al. [12] defines the expected score under q when the probabilistic prediction is p as the following form

$$S(p, q) = \int S(p, w) dq(w).$$

For simplicity, the score can be written as $S(\mathbf{x})$. Practically, logits or features from the penultimate layer are usually leveraged to calculate the score. Thus, for a given sample $\mathbf{x} \in \mathcal{X}$, $S(\cdot)$ is a function of $h(g(\mathbf{x}))$ and $g(\mathbf{x})$.

4 Outlier Aware Metric Learning

Our OAML training framework is shown in Figure 2. It primarily addresses the following issues: (1) how to effectively collect and train with outliers (Section 4.1); (2) how to mitigate the degradation of ID performance during OOD data training (Section 4.2).

4.1 Distribution-Assumption Free Latent Space Outlier Sampling

To synthesize OOD data for training models without assuming any distribution assumption in the latent space, we develop a method using k-NN and Stable Diffusion (SD) to generate large quantities of OOD features as the auxiliary dataset for outlier exposure training, thereby enhancing OOD detection performance to a great extent.

Coarse OOD Embeddings Sampling by k-NN. We first use the k-NN algorithm to sample outliers from the ID feature extracted by Vision Transformers [7] encoders mentioned in Figure 2. Different from NPOS [35] and DreamOOD [9], which sample OOD data from a well-trained text-conditioned latent space, we sample OOD embeddings in the Vision Transformers’ image embedding space. The reason is that the text-conditioned latent space is equivalent to a subspace of the image embedding space, which is smaller than the whole image embedding space. Therefore, extending the sampling space from the text-conditioned space

where $f^{out} \in \mathbb{R}^{H \times H}$ denotes the generated OOD embeddings which is the noisy feature map obtained at the T^{th} noise adding process, H is the size of the generated feature maps, \mathbf{x} is the input image. After the generation step, we flatten those generated OOD embeddings into long vectors as negative samples for contrastive learning.

Contrastive OOD Representation Learning. After obtaining all these coarse OOD embeddings and the generated OOD features mentioned above. Inspired by Cheng et al.’s work [3], we develop a mutual information-based outlier aware contrastive learning method to enlarge the discrepancy between ID and OOD feature distribution in semantic space. To be specific, we propose a loss function that minimizes the upper bound of mutual information between ID and OOD features. Different from [3], our method is an extension of their theory from the logits case to the feature case. Furthermore, we verify the non-trivial benefits of the OOD detection performance of our method in the experiments.

We use mutual information to quantify the distance between the ID and OOD feature distribution, which takes the form as follows,

$$I(f_S^{in}, f_T^{out}) = \mathbb{E}_{p(f_S^{in}, f_T^{out})} \left[\log \frac{p(f_S^{in}, f_T^{out})}{p(f_S^{in})p(f_T^{out})} \right],$$

where $f_S^{in} \in \mathbb{R}^m$ is the penultimate layer’s feature of the student network, $f_T^{out} \in \mathbb{R}^n$ is the OOD embeddings sampled by k-NN.

Then, the mutual information loss function can be written as

$$\begin{aligned} \hat{I}(f_S^{in}, f_T^{out}) &:= \mathcal{L}_{MI}(f_S^{in}; f_T^{out}) \\ &= \mathbb{E}_{p(f_S^{in}, f_T^{out})} [\log p(f_T^{out} | f_S^{in})] - \\ &\quad \mathbb{E}_{p(f_S^{in})} \mathbb{E}_{p(f_T^{out})} [\log p(f_T^{out} | f_S^{in})]. \end{aligned} \quad (1)$$

Indeed, one can easily show that $\hat{I}(f_S^{in}, f_T^{out})$ is an upper bound of $I(f_S^{in}, f_T^{out})$.

Theorem 1. $\hat{I}(f_S^{in}, f_T^{out})$ is an upper bound of $I(f_S^{in}, f_T^{out})$.

Additionally, we can show that the usage of the mutual information upper bound loss (1) for contrastive learning is not affected by the precision of upper bound estimates. This fact can be verified by Theorem 2. Detailed proof of Theorem 2 is given in the Appendix.

Theorem 2. Denote $I_{sup}(f_S^{in}, f_T^{out})$ as the supremum of $I(f_S^{in}, f_T^{out})$. If the amount of training data is large enough, then it is equivalent to using I_{sup} or I as the loss function to train the student network. And it is the same for using \hat{I} .

To sum up, during the training phase, the total loss function can be expressed as follows:

$$\begin{aligned} \mathcal{L}_{total} &= \mathcal{L}_{CE}(y^S, y^{gt}) + \alpha_1 \mathcal{L}_{KL}^1(y^S, y^T) \\ &\quad + \alpha_2 \mathcal{L}_{KL}^2(f_S^{in}, f_T^{in}) + \beta \mathcal{L}_{MI}(f_S^{in}, f_T^{out}) \\ &\quad + \gamma \mathcal{L}_{MI}(f_S^{in}, f_G^{out}), \end{aligned} \quad (2)$$

Algorithm 1 The Whole Outlier Training and Detection Pipeline

Step 1. Use k-NN to sample coarse OOD embeddings from large model embedding space.

Step 2. Generate far-OOD embeddings via Stable Diffusion.

Step 3. Simultaneously load the ID data and the OOD (near-OOD and far-OOD) features obtained in Steps 1 and 2, and perform OOD-aware learning.

Step 4. Use the features and logits of the network obtained after outlier exposure training to calculate the OOD score.

where f_G^{out} is the generated out-of-distribution embeddings through Stable Diffusion, $\alpha_1, \alpha_2, \beta, \gamma$ is the weight of each part of \mathcal{L}_{total} , \mathcal{L}_{CE} is the cross-entropy loss, \mathcal{L}_{KL}^1 is the KL-divergence loss for the logits output of student and teacher network, \mathcal{L}_{KL}^2 is the KL-divergence loss for the feature output of student and teacher network. The whole pipeline is summarized in Algorithm 1.

4.2 Knowledge Distillation for In-Distribution Performance Boosting

To prevent in-distribution classification accuracy from degradation and further enhance OOD detection performance. We develop a simple yet effective knowledge distillation method to transfer both logits and feature information from a large teacher model, simultaneously.

Specifically, we first use KL divergence loss to allow the student network to mimic the teacher network logits outputs, which can be formulated as follows:

$$\mathcal{L}_{KL}^1(y^S, y^T) = \int_{x \in \mathcal{X}} \ln \left(\frac{y^S}{y^T} \right) y^S dx, \quad (3)$$

where y^S is the logits prediction of student network, y^T is the prediction of teacher model, y^{gt} is the ground truth, f_S^{in} is the In-Distribution feature of student model, f_T^{in} is the ID feature extracted by teacher model.

Then, to transfer ID information at the features level, we use a domain transfer network consisting of a stack of Multilayer Perceptron (MLP) layers to align the feature spaces of the teacher model’s and student model’s penultimate layers. Formally, we denote the MLP transfer network as `linear`(\cdot). The learning object function for minimizing the distribution discrepancy between the teacher model’s feature and the student model’s feature can be written as follows:

$$\mathcal{L}_{KL}^2(f_S^{in}, f_T^{in}) = \int_{x \in \mathcal{X}} \ln \left(\frac{f_S^{in}}{\text{linear}(f_T^{in})} \right) f_S^{in} dx.$$

5 Experiments

5.1 ID and OOD Datasets.

We use CIFAR-10/100 [20] and ImageNet-1k [5] as ID datasets to train our models, respectively.

For OOD data preparation, when using CIFAR-10 [20] as the in-distribution dataset, we use CIFAR-100 [20], MNIST [6], SVHN [27] as the OOD datasets, in which CIFAR-100 [20] is the near-OOD datasets, MNIST [6], SVHN [27] are the far-OOD datasets. While using CIFAR-100 [20] as the ID dataset, we use CIFAR-10 [20], MNIST [6], SVHN [27] as the OOD datasets, where CIFAR-10 [20] is the near-OOD datasets, MNIST [6], SVHN [27] are the far-OOD datasets. What’s more, while using ImageNet-1k [5] as the ID dataset and we let SSB-Hard [37], NINCO [1], Inatralist [36], Textures [4], OpenImageO [38].

5.2 Evaluation metrics.

To evaluate the ability to detect out-of-distribution (OOD) examples, we use the False Positive Rate at 95% True Positive Rate (FPR95) and the Area Under the Receiver Operating Characteristic curve (AUROC). Lower FPR95 values and higher AUROC values indicate better OOD detection performance. Additionally, we report the in-distribution classification accuracy (ID ACC) of the tested models.

5.3 Implementation details.

We choose ResNet-18 [13] as the the student model, ViT-16 [7] as the teacher model. Our models are trained and evaluated utilizing a single NVIDIA Tesla V100 SMX2 32GB GPU. Our code is based on OpenOOD [45]. The resolution of both train and test images are 224×224 . For the CIFAR-10 dataset [20], our proposed OAML learning pipeline is configured with 500 epochs, leveraging pre-trained weights and a learning rate of 0.001. A comprehensive list of other hyperparameters can be found in the Appendix. When conducting experiments on CIFAR-100 [20], we set the learning rate as 0.01 and the epoch as 500, the other hyperparameters are given in the Appendix. For the experiments on ImageNet-1k [5], we only use 50 epochs for training and the learning rate is 5×10^{-5} . What’s more, **we do not employ any test time augmentation or data augmentation techniques.**

5.4 Main Results

In our experiments, to verify the universality and the effectiveness of our methods, we apply OAML to the energy-based [23], distance-based [33], and softmax-based [24] scores, respectively. All results on each OOD dataset and their averages are shown in Table 1, Table 2, and Table 3.

Results on CIFAR-100. It is important to observe the results presented in Table 1 that the comparison between the original EBO [23] and the EBO enhanced via OAML (as shown in the bottom row of Table 1) reveals significant improvements. Specifically, the EBO with OAML enhancement surpasses its unenhanced results by an average of 4.56% in FPR95, 3.11% in AUROC, and 2.12% in ID ACC on the CIFAR-100 dataset [20]. This enhancement is further

Table 1: Here we use CIFAR-100 [20] as in-distribution dataset to train a ResNet-18 [13] and make OOD test on the other three datasets. \uparrow indicates the higher the value, the better the OOD performance and vice versa.

Methods	Near-OOD		OOD Dataset						ID ACC
	CIFAR-10		MNIST		SVHN		Average		
	FPR@95 \downarrow	AUROC \uparrow	FPR@95 \downarrow	AUROC \uparrow	FPR@95 \downarrow	AUROC \uparrow	FPR@95 \downarrow	AUROC \uparrow	
<i>Train without Outliers</i>									
MSP [16]	58.66	78.88	48.37	80.25	46.91	84.38	51.31	81.17	76.22
ODIN [22]	61.22	77.85	35.20	88.01	54.39	80.81	50.27	82.22	76.22
MDS [21]	78.50	61.66	69.63	64.71	78.24	57.86	75.46	61.41	75.99
KLM [15]	84.68	72.65	68.80	80.89	86.50	77.79	79.99	77.11	76.22
Gram [30]	92.94	50.30	94.72	41.75	11.47	97.51	66.38	63.19	76.22
ReAct [32]	71.14	73.38	58.37	77.55	34.28	89.22	54.60	80.05	75.36
GradNorm [30]	73.16	75.50	59.80	79.75	28.37	91.11	53.78	82.12	76.22
ViM [38]	65.58	70.96	56.06	74.05	63.04	69.03	61.56	71.35	76.22
KNN [33]	71.80	76.19	46.34	84.69	56.16	85.12	58.10	82.00	76.22
GEN [24]	60.82	78.44	46.44	81.36	38.76	87.47	48.67	82.42	76.22
EBO [23]	60.84	78.43	46.43	81.36	38.73	87.48	48.67	82.42	76.22
<i>Train with Outliers</i>									
KNN w/ OE	88.08	71.84	38.77	89.01	50.20	88.62	59.02	83.16	75.49
GEN w/ OE	61.01	78.39	39.59	86.20	49.28	85.22	49.96	83.27	75.49
EBO w/ OE [17]	65.78	77.14	37.13	87.96	37.82	88.63	46.91	84.57	75.49
KNN w/ MixOE	63.56	77.44	48.72	77.23	43.56	90.64	51.95	81.77	74.36
GEN w/ MixOE	64.41	76.25	40.76	86.82	30.93	91.92	45.37	85.00	74.36
EBO w/ MixOE [44]	64.49	76.24	40.73	86.84	30.90	91.93	45.37	85.00	74.36
KNN w/ OAML (Ours)	70.34	78.48	46.16	86.87	42.81	88.65	53.10	84.67	78.34
GEN w/ OAML (Ours)	54.61	81.17	33.21	89.40	44.63	85.97	44.15	85.51	78.34
EBO w/ OAML (Ours)	54.58	81.17	33.14	89.42	44.60	85.99	44.11	85.53	78.34

validated when comparing EBO trained by our OAML method against the basic OE methods [17], we find that our OAML enhancement is stronger than OE [17]. Similar improvements are observed when comparing the KNN [33], the KNN trained by OE [17], and the KNN trained by OAML. Moreover, the EBO with OAML enhancement not only outperforms these models but also exceeds the state-of-the-art methods, including ViM [38], KNN [33], and GEN [24].

Evaluation on CIFAR-10. In Table 2, a comparison between EBO [24] and EBO augmented by OAML on the CIFAR-10 dataset [20] reveals that the latter achieves a notable enhancement, with an average reduction of 5.96% in FPR95 and an average increase of 1.62% in AUROC. This suggests that our OAML training approach significantly improves the original OOD detection performance, in contrast to the OE-based method, which yields minimal improvements and even declines in AUROC and ID ACC metrics. Similar findings are observed when examining the performance of KNN, both with and without OE training, as well as with OAML training.

By synthesizing the results depicted in Tables 1 and 2, it becomes evident that our methodology excels in augmenting the performance on far-OOD datasets, as exemplified by the studies in [6, 27]. For instance, as illustrated in Table 1, when comparing the EBO [23] with the EBO that has applied OAML training, we observe a substantial reduction in the FPR95 from 46.43% to 33.14%, along with a marked enhancement in the AUROC from 81.36% to 89.42% on the MNIST dataset [6]. In a parallel analysis, as presented in Table 2, the FPR95 is notably decreased from 19.68% to 6.91%, and the AUROC is significantly elevated from

Table 2: In this table, we use CIFAR-10 [20] as in-distribution dataset to train a ResNet-18 [13] and make OOD test on the other three datasets. \uparrow indicates the higher the value, the better the OOD performance and vice versa.

Methods	OOD Dataset								ID ACC
	Near-OOD CIFAR-100		MNIST		SVHN		Average		
	FPR@95 \downarrow	AUROC \uparrow	FPR@95 \downarrow	AUROC \uparrow	FPR@95 \downarrow	AUROC \uparrow	FPR@95 \downarrow	AUROC \uparrow	
<i>Train without Outliers</i>									
MSP [16]	34.81	89.52	22.74	92.94	16.81	94.48	24.79	92.31	94.66
ODIN [22]	47.94	87.87	10.77	97.52	24.26	94.38	27.66	93.26	94.66
KLM [15]	85.77	80.18	80.89	84.89	82.98	85.72	83.21	83.60	94.66
Gram [30]	86.66	64.63	86.82	46.07	10.64	97.60	61.37	69.43	94.66
GradNorm [30]	71.61	79.87	41.28	88.65	25.59	93.37	46.16	87.30	94.66
ViM [38]	37.39	88.74	17.06	95.84	21.52	91.19	25.32	91.92	94.66
ReAct [32]	40.78	89.67	23.13	94.06	14.63	96.05	26.18	93.26	94.64
KNN [33]	37.43	89.44	23.31	93.45	26.63	91.48	29.12	91.46	94.66
GEN [24]	34.38	90.65	19.98	94.68	12.70	96.53	22.35	93.95	94.66
EBO [23]	34.40	90.65	19.68	94.74	12.27	96.59	22.12	93.99	94.66
<i>Train with Outliers</i>									
KNN w/ OE	38.44	89.33	28.46	91.21	27.94	91.23	31.61	90.59	94.36
GEN w/ OE	33.46	89.97	17.74	95.07	13.59	96.55	21.60	93.86	94.36
EBO w/ OE [17]	32.56	91.19	12.76	97.24	9.03	98.04	18.12	95.49	94.36
KNN w/ MixOE	39.49	88.52	17.89	95.18	26.44	91.16	27.94	91.62	93.83
GEN w/ MixOE	37.44	89.42	14.80	96.64	24.59	91.66	25.61	92.57	93.83
EBO w/ MixOE [44]	38.62	89.17	12.24	97.15	27.42	90.27	26.09	92.20	93.83
KNN w/ OAML (Ours)	33.52	90.74	15.59	94.95	14.68	94.57	21.26	93.42	94.89
GEN w/ OAML (Ours)	31.60	91.68	7.07	98.12	10.09	96.98	16.25	95.59	94.89
EBO w/ OAML (Ours)	31.54	91.68	6.91	98.15	10.06	96.99	16.16	95.61	94.89

94.74% to 98.15% on the same MNIST dataset [6]. These findings underscore the superior efficacy of our approach in refining OOD detection accuracy, particularly in scenarios where the dataset deviates markedly from the model’s training distribution. The same conclusions can be obtained by comparing our method with MixOE [44].

Evaluation on ImageNet-1k. We also performed extensive experiments utilizing the ImageNet-1k [5] dataset as an ID training dataset, with the comprehensive results delineated in Table 3. A thorough examination of the data presented in Table 3 demonstrates that our OAML method substantially improves the performance of distance-based score functions. This enhancement is particularly evident in KNN [33], where the FPR95 is notably reduced from 54.77% to 52.95%, and the AUROC is significantly elevated from 79.51% to 81.91%. Furthermore, the ID ACC is also improved after using our OAML approach.

Moreover, we conduct comparisons between OAML and the other outlier synthesis-based methods, such as VOS [11], NPOS [35], DreamOOD [10], and ATOL [46], in Table 4. These comparisons further demonstrate the advantages of our method.

5.5 Ablation Analysis

Learning Loss Comparison. In this section, we compare the validation loss of DreamOOD [9], VOS [11], and OAML in Figure 3, to show that synthesizing outliers in the feature space is better than synthesizing in pixel space. From subplot (a) and (b) in Figure 3 we can see that both the loss value of VOS

Table 3: In this Table, we use ImageNet-1k [5] as in-distribution dataset to train a ResNet-18 [13] and make OOD test on the other five datasets. \uparrow indicates the higher the value, the better the OOD performance and vice versa.

Methods	OOD Dataset												ID ACC
	Near-OOD				Par-OOD				Average				
	SSB-HARD		NINCO		INaturalist		Textures		OpenImageO		Average		
	FPR@95 \downarrow	AUROC \uparrow	FPR@95 \downarrow	AUROC \uparrow	FPR@95 \downarrow	AUROC \uparrow	FPR@95 \downarrow	AUROC \uparrow	FPR@95 \downarrow	AUROC \uparrow	FPR@95 \downarrow	AUROC \uparrow	
<i>Train without Outliers</i>													
MSP [16]	74.49	72.09	56.88	79.95	43.34	88.41	60.87	82.43	50.13	84.86	57.14	81.55	76.18
ODIN [22]	76.83	71.74	68.20	77.77	35.98	91.17	49.24	89.00	46.66	88.23	55.38	83.58	76.20
KLM [13]	84.71	71.38	60.36	81.90	38.52	90.78	52.40	84.72	48.89	87.30	56.98	83.22	76.18
ReAct [23]	77.55	73.03	55.82	81.73	16.72	96.34	29.61	92.79	32.58	91.87	42.46	87.16	73.58
VIM [18]	79.59	65.88	59.08	78.80	32.70	86.72	17.22	96.65	33.74	88.96	44.47	83.40	76.18
KNN [33]	84.45	60.95	60.02	77.85	53.21	78.60	24.13	96.09	51.13	84.05	54.77	79.51	76.18
GEN [24]	75.73	72.01	54.90	81.70	26.10	92.44	46.22	87.59	34.50	89.26	47.49	84.60	76.18
<i>Train with Outliers</i>													
KNN w/ OAML (Ours)	87.43	61.94	66.41	77.03	39.80	89.07	17.14	97.05	53.97	84.44	52.95	81.91	77.12
GEN w/ OAML (Ours)	77.77	71.93	54.75	82.18	30.29	90.92	46.80	86.55	38.56	87.88	49.63	83.89	77.12

Table 4: Comparison with state-of-the-art Outlier Synthesis Methods, wherein we take CIFAR-100 [20] as the ID dataset.

Methods	OOD Dataset					
	CIFAR-10		SVHN		Average	
	FPR@95 \downarrow	AUROC \uparrow	FPR@95 \downarrow	AUROC \uparrow	FPR@95 \downarrow	AUROC \uparrow
VOS [11]	62.17	78.93	61.68	78.10	61.93	78.52
NPOS [35]	91.29	53.14	93.63	65.23	92.46	72.80
DreamOOD [9]	79.70	78.89	59.05	86.78	69.38	82.84
ATOL [46]	82.55	73.28	72.30	81.82	77.43	77.55
OAML (Ours)	54.58	81.17	44.60	85.99	49.59	83.58

and OAML (using outliers sampled from the feature space) are smaller than DreamOOD’s loss value, which means that using pixel level OOD data for training is not easy to optimize. This fact further verifies the statements in VOS [11]. Furthermore, in subplot (c) in Figure 3, we can see that OAML’s loss value is also smaller than VOS. This fact implies that OAML learns better than the other outlier synthesis-based methods.

OOD Verification for the Generated Data. Here we verify whether the data generated by Diffusion are truly out-of-distribution by calculating the KL-Divergence value between the synthesized outliers and the in-distribution features extracted by ResNets. The visualization of KL value comparison is shown in Figure 4. We can see that the outliers sampled by SD (D-OOD) achieve the highest KL-value among all benchmarks and the OOD data sampled by k-NN (C-OOD) achieve the second highest KL-value, which means that the data distribution between D-OOD and ID data distribution has the farthest distance than the other three kinds of OOD data shown in the figure.

Moreover, in Figure 5, we use K-means [25] for clustering ID and OOD components in the generated data. We can see that the ID and OOD feature distribution of the Diffusion generated outliers are more separable than those sampled by vanilla k-NN.

Ablation for Loss Function. In this section, we delve into the impact of various training loss terms outlined in Equation 2, which are predicated on the GEN [24] score and EBO [23] score. The results are shown in Table 5. A comparative

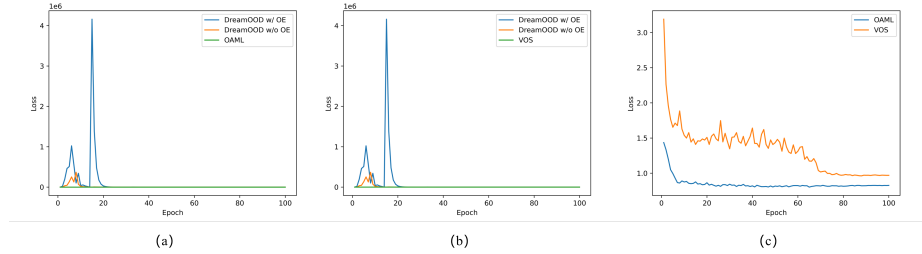


Fig. 3: The loss comparison between DreamOOD [9] and VOS [11] and OAML (Ours) when performing Outlier Exposure training **under the same training settings**.

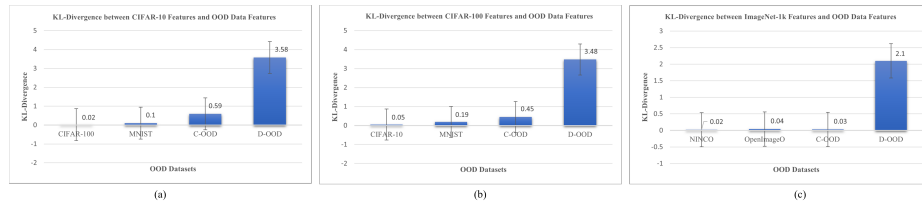


Fig. 4: The KL Divergence value between ID and OOD data pairs using CIFAR-10/100 [20], ImageNet-1k [5] as ID data, respectively. In each subplot, C-OOD refers to outliers generated by k-NN ($k=30$) and D-OOD refers to outliers sampled by Stable Diffusion [29].

analysis between the first and final rows of Table 5 reveals that our OAML training methodologies have successfully enhanced the GEN score by an average of 4.52% at FPR95 and 3.09% in AUROC. Concurrently, there is a notable improvement in the ID ACC metric as well. The ablation study conducted on the EBO [23] score yields similar findings.

More importantly, by comparing the first row and the second row in Table 1 we can see that our knowledge distillation methods boost the ID classification accuracy on both EBO [23] and GEN [24]. Besides, we find that this technique prevents ID accuracy degradation even after the OOD samples are introduced for training.

Score Distribution Ablation. For a more comprehensive analysis, the comparative visualization of EBO’s score distribution on CIFAR-10 [20], when trained by OE [17] and our proposed OAML framework, is presented in Figure 6 for further examination. By examining the first and final rows in Figure 6, it becomes evident that the application of our OAML framework results in a discernible reduction in the overlap between the In-Distribution (ID) and Out-Of-Distribution (OOD) score distributions. This diminished overlap is indicative of an enhanced

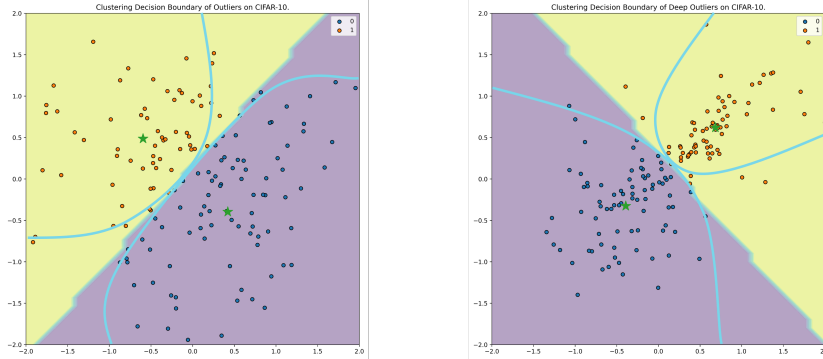


Fig. 5: The decision boundary visualization of clustering the selected outliers generated via k-NN and Stable Diffusion on CIFAR-10 [20], respectively. The green stars are the clustering center of ID (labeled as 0) and OOD (labeled as 1) data of the generated OOD embeddings. The subplot (a) is the decision boundary of clustered outliers generated by k-NN and subplot (b) is the decision boundary of clustered outliers further generated by Stable Diffusion [29].

OOD detection capability, signifying an improvement in the model’s ability to distinguish between ID and OOD data. Then, a comparison between the second and the last row reveals that our OAML algorithm further diminishes the overlap between the ID and OOD score distributions compared to OE, this phenomenon is particularly significant in the far-OOD dataset. Besides, we can also see that the variance of the estimated scores on both ID and OOD data are reduced considerably after applying OAML, which shows the great enhancing power of our method.

Table 5: Ablation studies for our learning framework on GEN score [24] and EBO score [23]. Here we use CIFAR-100 [20] as the ID dataset to train our network. In the table below, \uparrow indicates the higher the value, the better the OOD performance, and vice versa.

Method	Feature and Logits Distillation	Contrstive Outlier Exposure	Deep Contrstive Outlier Exposure	FPR@95(\downarrow)	AUROC (\uparrow)	ID ACC(%)
GEN [24]	✓			48.67	82.42	76.22
	✓			50.39	83.49	78.38
	✓	✓		44.73	84.94	78.32
	✓	✓	✓	44.15	85.51	78.34
EBO [23]	✓			48.67	82.42	76.22
	✓			50.31	83.50	78.38
	✓	✓		50.73	83.27	77.54
	✓	✓	✓	44.11	85.53	78.34

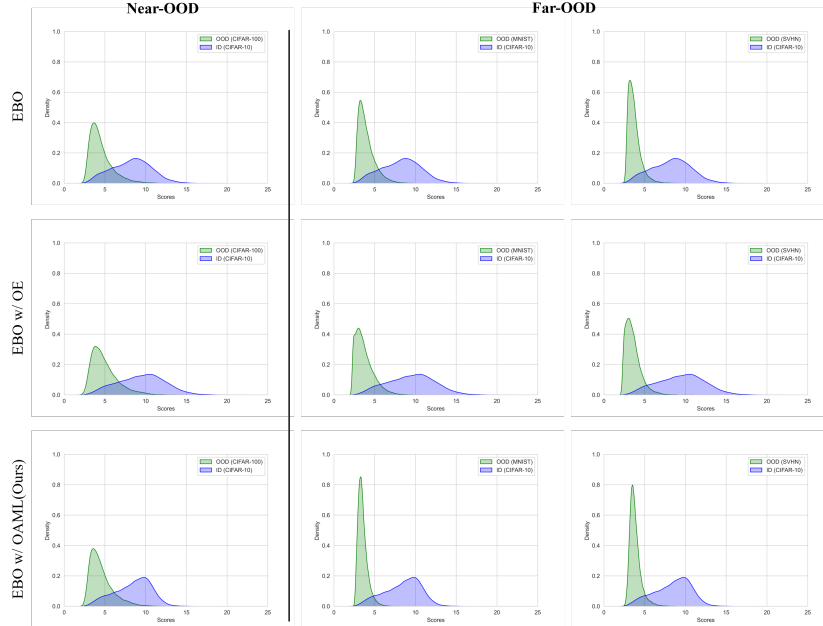


Fig. 6: The score distribution visualization of EBO [23] which takes CIFAR-10 [20] as the ID data. The first row of the above figure is the energy score distribution taking ResNet-18 [13] as the backbone. The second row is the ResNet-18 [13] trained by OE. The third row is the ResNet-18 [13] trained by OAML.

6 Conclusion

In this work, we develop a novel outlier exposure training framework, dubbed OAML, for enhancing OOD detection performance. We believe that the main challenge in OE training lies in how to collect and learn from OOD samples. Thus, our training pipeline first uses k-NN and Stable Diffusion to generate outliers in the latent space without making any distributional assumptions. Then, we design a mutual information-based contrastive learning approach to enlarge the distance between ID and OOD data distribution in the semantic space, guaranteed by both theoretical and empirical results. Moreover, we introduce knowledge distillation to prevent ID performance from decreasing when training with the mixture of ID and OOD data. Our experiments exhibit non-trivial improvements across different kinds of score functions on various benchmarks, demonstrating the effectiveness of our learning framework for OOD detection performance enhancement.

References

1. Bitterwolf, J., Müller, M., Hein, M.: In or out? fixing imagenet out-of-distribution detection evaluation. arXiv preprint arXiv:2306.00826 (2023) [8](#)
2. Chen, T., Kornblith, S., Norouzi, M., Hinton, G.: A simple framework for contrastive learning of visual representations. In: International conference on machine learning. pp. 1597–1607. PMLR (2020) [3](#)
3. Cheng, P., Hao, W., Dai, S., Liu, J., Gan, Z., Carin, L.: Club: A contrastive log-ratio upper bound of mutual information. In: International conference on machine learning. pp. 1779–1788. PMLR (2020) [6](#)
4. Cimpoi, M., Maji, S., Kokkinos, I., Mohamed, S., Vedaldi, A.: Describing textures in the wild. In: Proceedings of the IEEE conference on computer vision and pattern recognition. pp. 3606–3613 (2014) [8](#)
5. Deng, J., Dong, W., Socher, R., Li, L.J., Li, K., Fei-Fei, L.: Imagenet: A large-scale hierarchical image database. In: 2009 IEEE conference on computer vision and pattern recognition. pp. 248–255. Ieee (2009) [2](#), [3](#), [7](#), [8](#), [10](#), [11](#), [12](#), [18](#), [19](#)
6. Deng, L.: The mnist database of handwritten digit images for machine learning research [best of the web]. IEEE signal processing magazine **29**(6), 141–142 (2012) [8](#), [9](#), [10](#)
7. Dosovitskiy, A., Beyer, L., Kolesnikov, A., Weissenborn, D., Zhai, X., Unterthiner, T., Dehghani, M., Minderer, M., Heigold, G., Gelly, S., et al.: An image is worth 16x16 words: Transformers for image recognition at scale. In: International Conference on Learning Representations (2020) [4](#), [8](#)
8. Du, X., Gozum, G., Ming, Y., Li, Y.: Siren: Shaping representations for detecting out-of-distribution objects. Advances in Neural Information Processing Systems **35**, 20434–20449 (2022) [3](#)
9. Du, X., Sun, Y., Zhu, J., Li, Y.: Dream the impossible: Outlier imagination with diffusion models. In: Oh, A., Naumann, T., Globerson, A., Saenko, K., Hardt, M., Levine, S. (eds.) Advances in Neural Information Processing Systems. vol. 36, pp. 60878–60901. Curran Associates, Inc. (2023), https://proceedings.neurips.cc/paper_files/paper/2023/file/bf5311df07f3efce97471921e6d2f159-Paper-Conference.pdf [2](#), [3](#), [4](#), [10](#), [11](#), [12](#)
10. Du, X., Wang, X., Gozum, G., Li, Y.: Unknown-aware object detection: Learning what you don’t know from videos in the wild. In: Proceedings of the IEEE/CVF Conference on Computer Vision and Pattern Recognition. pp. 13678–13688 (2022) [10](#)
11. Du, X., Wang, Z., Cai, M., Li, Y.: Vos: Learning what you don’t know by virtual outlier synthesis. arXiv preprint arXiv:2202.01197 (2022) [1](#), [2](#), [3](#), [10](#), [11](#), [12](#)
12. Gneiting, T., Raftery, A.E.: Strictly proper scoring rules, prediction, and estimation. Journal of the American statistical Association **102**(477), 359–378 (2007) [4](#)
13. He, K., Zhang, X., Ren, S., Sun, J.: Deep residual learning for image recognition. In: Proceedings of the IEEE conference on computer vision and pattern recognition. pp. 770–778 (2016) [8](#), [9](#), [10](#), [11](#), [14](#), [19](#)
14. Hendrycks, D., Basart, S., Mazeika, M., Zou, A., Kwon, J., Mostajabi, M., Steinhardt, J., Song, D.: Scaling out-of-distribution detection for real-world settings. arXiv preprint arXiv:1911.11132 (2019) [1](#)
15. Hendrycks, D., Basart, S., Mazeika, M., Zou, A., Kwon, J., Mostajabi, M., Steinhardt, J., Song, D.: Scaling out-of-distribution detection for real-world settings. In: International Conference on Machine Learning. pp. 8759–8773. PMLR (2022) [9](#), [10](#), [11](#)

16. Hendrycks, D., Gimpel, K.: A baseline for detecting misclassified and out-of-distribution examples in neural networks. arXiv preprint arXiv:1610.02136 (2016) [9](#), [10](#), [11](#)
17. Hendrycks, D., Mazeika, M., Dietterich, T.: Deep anomaly detection with outlier exposure. In: International Conference on Learning Representations (2018) [1](#), [2](#), [3](#), [9](#), [10](#), [12](#)
18. Hsu, Y.C., Shen, Y., Jin, H., Kira, Z.: Generalized odin: Detecting out-of-distribution image without learning from out-of-distribution data. In: Proceedings of the IEEE/CVF Conference on Computer Vision and Pattern Recognition. pp. 10951–10960 (2020) [1](#)
19. Kramer, O., Kramer, O.: K-nearest neighbors. Dimensionality reduction with unsupervised nearest neighbors pp. 13–23 (2013) [2](#)
20. Krizhevsky, A., Hinton, G., et al.: Learning multiple layers of features from tiny images (2009) [2](#), [3](#), [7](#), [8](#), [9](#), [10](#), [11](#), [12](#), [13](#), [14](#), [18](#), [19](#), [26](#)
21. Lee, K., Lee, K., Lee, H., Shin, J.: A simple unified framework for detecting out-of-distribution samples and adversarial attacks. Advances in neural information processing systems **31** (2018) [9](#)
22. Liang, S., Li, Y., Srikant, R.: Enhancing the reliability of out-of-distribution image detection in neural networks. arXiv preprint arXiv:1706.02690 (2017) [1](#), [9](#), [10](#), [11](#)
23. Liu, W., Wang, X., Owens, J., Li, Y.: Energy-based out-of-distribution detection. Advances in neural information processing systems **33**, 21464–21475 (2020) [1](#), [8](#), [9](#), [10](#), [11](#), [12](#), [13](#), [14](#)
24. Liu, X., Lochman, Y., Zach, C.: Gen: Pushing the limits of softmax-based out-of-distribution detection. In: Proceedings of the IEEE/CVF Conference on Computer Vision and Pattern Recognition. pp. 23946–23955 (2023) [2](#), [8](#), [9](#), [10](#), [11](#), [12](#), [13](#)
25. MacQueen, J., et al.: Some methods for classification and analysis of multivariate observations. In: Proceedings of the fifth Berkeley symposium on mathematical statistics and probability. vol. 1, pp. 281–297. Oakland, CA, USA (1967) [11](#)
26. Ming, Y., Sun, Y., Dia, O., Li, Y.: How to exploit hyperspherical embeddings for out-of-distribution detection? arXiv preprint arXiv:2203.04450 (2022) [1](#)
27. Netzer, Y., Wang, T., Coates, A., Bissacco, A., Wu, B., Ng, A.Y.: Reading digits in natural images with unsupervised feature learning (2011) [8](#), [9](#)
28. Radford, A., Kim, J.W., Hallacy, C., Ramesh, A., Goh, G., Agarwal, S., Sastry, G., Askell, A., Mishkin, P., Clark, J., et al.: Learning transferable visual models from natural language supervision. In: International conference on machine learning. pp. 8748–8763. PMLR (2021) [3](#)
29. Rombach, R., Blattmann, A., Lorenz, D., Esser, P., Ommer, B.: High-resolution image synthesis with latent diffusion models. In: Proceedings of the IEEE/CVF conference on computer vision and pattern recognition. pp. 10684–10695 (2022) [2](#), [3](#), [5](#), [12](#), [13](#), [26](#)
30. Sastry, C.S., Oore, S.: Detecting out-of-distribution examples with gram matrices. In: International Conference on Machine Learning. pp. 8491–8501. PMLR (2020) [9](#), [10](#)
31. Sehwal, V., Chiang, M., Mittal, P.: Ssd: A unified framework for self-supervised outlier detection. arXiv preprint arXiv:2103.12051 (2021) [1](#), [3](#)
32. Sun, Y., Guo, C., Li, Y.: React: Out-of-distribution detection with rectified activations. Advances in Neural Information Processing Systems **34**, 144–157 (2021) [9](#), [10](#), [11](#)
33. Sun, Y., Ming, Y., Zhu, X., Li, Y.: Out-of-distribution detection with deep nearest neighbors. In: International Conference on Machine Learning. pp. 20827–20840. PMLR (2022) [2](#), [8](#), [9](#), [10](#), [11](#)

34. Tack, J., Mo, S., Jeong, J., Shin, J.: Csi: Novelty detection via contrastive learning on distributionally shifted instances. *Advances in neural information processing systems* **33**, 11839–11852 (2020) [3](#)
35. Tao, L., Du, X., Zhu, J., Li, Y.: Non-parametric outlier synthesis. In: *The Eleventh International Conference on Learning Representations* (2022) [3](#), [4](#), [10](#), [11](#)
36. Van Horn, G., Mac Aodha, O., Song, Y., Cui, Y., Sun, C., Shepard, A., Adam, H., Perona, P., Belongie, S.: The inaturalist species classification and detection dataset. In: *Proceedings of the IEEE conference on computer vision and pattern recognition*. pp. 8769–8778 (2018) [8](#)
37. Vaze, S., Han, K., Vedaldi, A., Zisserman, A.: Open-set recognition: A good closed-set classifier is all you need? *arXiv preprint arXiv:2110.06207* (2021) [8](#)
38. Wang, H., Li, Z., Feng, L., Zhang, W.: Vim: Out-of-distribution with virtual-logit matching. In: *Proceedings of the IEEE/CVF conference on computer vision and pattern recognition*. pp. 4921–4930 (2022) [8](#), [9](#), [10](#), [11](#)
39. Wei, H., Xie, R., Cheng, H., Feng, L., An, B., Li, Y.: Mitigating neural network overconfidence with logit normalization. In: *International Conference on Machine Learning*. pp. 23631–23644. PMLR (2022) [18](#), [19](#)
40. Winkens, J., Bunel, R., Roy, A.G., Stanforth, R., Natarajan, V., Ledsam, J.R., MacWilliams, P., Kohli, P., Karthikesalingam, A., Kohl, S., et al.: Contrastive training for improved out-of-distribution detection. *arXiv preprint arXiv:2007.05566* (2020) [1](#), [3](#)
41. Yang, J., Wang, H., Feng, L., Yan, X., Zheng, H., Zhang, W., Liu, Z.: Semantically coherent out-of-distribution detection. In: *Proceedings of the IEEE/CVF International Conference on Computer Vision*. pp. 8301–8309 (2021) [18](#), [19](#)
42. Yang, J., Zhou, K., Li, Y., Liu, Z.: Generalized out-of-distribution detection: A survey. *arXiv preprint arXiv:2110.11334* (2021) [2](#)
43. Yu, Q., Aizawa, K.: Unsupervised out-of-distribution detection by maximum classifier discrepancy. In: *Proceedings of the IEEE/CVF international conference on computer vision*. pp. 9518–9526 (2019) [1](#), [18](#), [19](#)
44. Zhang, J., Inkawhich, N., Linderman, R., Chen, Y., Li, H.: Mixture outlier exposure: Towards out-of-distribution detection in fine-grained environments. In: *Proceedings of the IEEE/CVF Winter Conference on Applications of Computer Vision*. pp. 5531–5540 (2023) [9](#), [10](#)
45. Zhang, J., Yang, J., Wang, P., Wang, H., Lin, Y., Zhang, H., Sun, Y., Du, X., Zhou, K., Zhang, W., Li, Y., Liu, Z., Chen, Y., Li, H.: Openood v1.5: Enhanced benchmark for out-of-distribution detection. *arXiv preprint arXiv:2306.09301* (2023) [8](#)
46. Zheng, H., Wang, Q., Fang, Z., Xia, X., Liu, F., Liu, T., Han, B.: Out-of-distribution detection learning with unreliable out-of-distribution sources. *Advances in Neural Information Processing Systems* **36** (2024) [10](#), [11](#)

A Appendix

In this appendix, we elucidate the training configurations of OAML and augment our analysis with additional experiments. These new experiments serve to contrast our approach with various training-based Out-of-Distribution (OOD) detection methods. Furthermore, we provide proof for the theorems outlined in our original manuscript and offer a theoretical justification for the efficacy of OAML.

A.1 OAML Training Settings

Here we give the values of hyperparameters used in our loss function \mathcal{L}_{total} , readers may check the value of the hyperparameters in Table 6. The hyperparameters on CIFAR-10 [20] are shown in Table 6. The hyperparameters on CIFAR-100 [20] are shown in Table 7. And the hyperparameters on ImageNet-1k [5] are presented in Table 8.

Table 6: The hyperparameters for using our OAML framework on CIFAR-10 [20].

Hyperparameters	Value
α_1	4.0
α_2	8.0
β	0.1
γ	0.2

Table 7: The hyperparameters for using our OAML framework on CIFAR-100 [20].

Hyperparameters	Value
α_1	4.0
α_2	8.0
β	0.1
γ	0.2

A.2 Comparisons between OAML and Other Training based OOD Detection Approaches

In this section, we compare OAML with other Outlier Exposure-based and training-based approaches like MCD [43], LogitNorm [39] and UDG [41]. The results are shown in Table 9 and 10.

Table 8: The hyperparameters for using our OAML framework on ImageNet-1k [5].

Hyperparameters	Value
α_1	4.0
α_2	8.0
β	0.1
γ	0.2

Table 9: Here we use CIFAR-100 [20] as in-distribution dataset to train a ResNet-18 [13] and make OOD test on the other three datasets. \uparrow indicates the higher the value, the better the OOD performance and vice versa.

Methods	OOD Dataset								ID ACC
	Near-OOD CIFAR-10		Far-OOD				Average		
	FPR@95 \downarrow	AUROC \uparrow	MNIST FPR@95 \downarrow	MNIST AUROC \uparrow	SVHN FPR@95 \downarrow	SVHN AUROC \uparrow	FPR@95 \downarrow	AUROC \uparrow	
KNN w/ MCD	86.79	72.81	29.73	90.85	70.31	83.70	62.28	82.45	75.61
GEN w/ MCD	62.81	78.08	46.29	84.86	49.93	83.40	53.01	82.11	75.61
EBO w/ MCD [43]	62.82	78.06	46.26	84.87	49.78	83.42	52.95	82.12	75.61
KNN w/ LogitNorm	97.24	60.31	30.48	88.48	8.63	98.35	45.45	82.38	74.98
GEN w/ LogitNorm	83.71	67.24	65.78	68.21	28.44	93.00	59.31	76.15	74.98
EBO w/ LogitNorm [39]	85.08	66.44	67.96	67.38	29.50	92.89	60.85	75.57	74.98
KNN w/ UDG	68.69	74.84	44.29	84.41	72.08	76.85	61.69	78.70	70.46
GEN w/ UDG	67.11	75.26	26.98	93.23	53.14	79.03	49.08	82.51	70.46
EBO w/ UDG [41]	67.12	75.26	26.97	93.24	53.14	79.03	49.08	82.51	70.46
KNN w/ OAML (Ours)	70.34	78.48	46.16	86.87	42.81	88.65	53.10	84.67	78.34
GEN w/ OAML (Ours)	54.61	81.17	33.21	89.40	44.63	85.97	44.15	85.51	78.34
EBO w/ OAML (Ours)	54.58	81.17	33.14	89.42	44.60	85.99	44.11	85.53	78.34

Table 10: Here we use CIFAR-10 [20] as in-distribution dataset to train a ResNet-18 [13] and make OOD test on the other three datasets. \uparrow indicates the higher the value, the better the OOD performance and vice versa.

Methods	OOD Dataset								ID ACC
	Near-OOD CIFAR-100		Far-OOD				Average		
	FPR@95 \downarrow	AUROC \uparrow	MNIST FPR@95 \downarrow	MNIST AUROC \uparrow	SVHN FPR@95 \downarrow	SVHN AUROC \uparrow	FPR@95 \downarrow	AUROC \uparrow	
KNN w/ MCD	38.31	89.12	23.60	93.16	29.93	90.93	30.61	91.07	94.16
GEN w/ MCD	34.01	90.55	24.48	92.70	14.92	95.83	24.47	93.03	94.16
EBO w/ MCD [43]	33.93	90.54	24.48	92.69	14.64	95.90	24.35	93.04	94.16
KNN w/ LogitNorm	37.58	89.34	24.14	93.06	23.70	92.26	28.47	91.55	94.60
GEN w/ LogitNorm	34.48	90.42	21.92	94.06	10.69	96.96	22.36	93.81	94.60
EBO w/ LogitNorm [39]	34.43	90.41	21.91	94.08	10.56	96.99	22.30	93.83	94.60
KNN w/ UDG	58.06	78.46	31.11	88.71	52.16	80.99	47.11	82.72	86.39
GEN w/ UDG	55.57	81.86	19.54	95.05	62.47	77.09	45.86	84.67	86.39
EBO w/ UDG [41]	56.00	81.82	19.42	95.09	62.51	77.05	45.98	84.65	86.39
KNN w/ OAML (Ours)	33.52	90.74	15.59	94.95	14.68	94.57	21.26	93.42	94.89
GEN w/ OAML (Ours)	31.60	91.68	7.07	98.12	10.09	96.98	16.25	95.59	94.89
EBO w/ OAML (Ours)	31.54	91.68	6.91	98.15	10.06	96.99	16.16	95.61	94.89

A.3 Proof for Theorem 1

Proof. Indeed, I and \hat{I} can be written as the following form,

$$\begin{aligned} I(f_S^{in}, f_T^{out}) &= \mathbb{E}_{p(f_S^{in}, f_T^{out})} \left[\log \frac{p(f_T^{out} | f_S^{in})}{p(f_T^{out})} \right], \\ \hat{I}(f_S^{in}, f_T^{out}) &= \mathbb{E}_{p(f_S^{in}, f_T^{out})} [\log p(f_T^{out} | f_S^{in})] - \mathbb{E}_{p(f_S^{in})} \mathbb{E}_{p(f_T^{out})} [\log p(f_T^{out} | f_S^{in})]. \end{aligned}$$

Denote $\Delta := \hat{I}(f_S^{in}, f_T^{out}) - I(f_S^{in}, f_T^{out})$. Then, we have

$$\begin{aligned} \Delta &= \mathbb{E}_{p(f_S^{in}, f_T^{out})} [\log p(f_T^{out} | f_S^{in})] - \mathbb{E}_{p(f_S^{in})} \mathbb{E}_{p(f_T^{out})} [\log p(f_T^{out} | f_S^{in})] \\ &\quad - \mathbb{E}_{p(f_S^{in}, f_T^{out})} \left[\log \frac{p(f_T^{out} | f_S^{in})}{p(f_T^{out})} \right] \\ &= \mathbb{E}_{p(f_S^{in}, f_T^{out})} [\log p(f_T^{out} | f_S^{in})] - \mathbb{E}_{p(f_S^{in})} \mathbb{E}_{p(f_T^{out})} [\log p(f_T^{out} | f_S^{in})] \\ &\quad - \mathbb{E}_{p(f_S^{in}, f_T^{out})} [\log p(f_T^{out} | f_S^{in})] + \mathbb{E}_{p(f_S^{in}, f_T^{out})} [\log p(f_T^{out})] \\ &= \mathbb{E}_{p(f_S^{in}, f_T^{out})} [\log p(f_T^{out})] - \mathbb{E}_{p(f_S^{in})} \mathbb{E}_{p(f_T^{out})} [\log p(f_T^{out} | f_S^{in})] \\ &= \int_{\mathbb{R}^d} df_S^{in} \int_{\mathbb{R}^d} \log p(f_T^{out}) p(f_S^{in}, f_T^{out}) df_T^{out} - \mathbb{E}_{p(f_S^{in})} \mathbb{E}_{p(f_T^{out})} [\log p(f_T^{out} | f_S^{in})] \\ &= \int_{\mathbb{R}^d} \log p(f_T^{out}) \left(\int_{\mathbb{R}^d} p(f_S^{in}, f_T^{out}) df_S^{in} \right) df_T^{out} - \\ &\quad \mathbb{E}_{p(f_S^{in})} \mathbb{E}_{p(f_T^{out})} [\log p(f_T^{out} | f_S^{in})] \\ &= \int_{\mathbb{R}^d} \log [p(f_T^{out})] p(f_T^{out}) df_T^{out} - \\ &\quad \int_{\mathbb{R}^d} p(f_S^{in}) df_S^{in} \int_{\mathbb{R}^d} \log [p(f_T^{out} | f_S^{in})] p(f_T^{out}) df_T^{out} \\ &= \int_{\mathbb{R}^d} \log [p(f_T^{out})] p(f_T^{out}) df_T^{out} - \\ &\quad \int_{\mathbb{R}^d} p(f_T^{out}) df_T^{out} \int_{\mathbb{R}^d} \log [p(f_T^{out} | f_S^{in})] p(f_S^{in}) df_S^{in} \\ &= \mathbb{E}_{p(f_T^{out})} [\log p(f_T^{out})] - \mathbb{E}_{p(f_T^{out})} \left[\mathbb{E}_{p(f_S^{in})} [\log p(f_T^{out} | f_S^{in})] \right] \\ &= \mathbb{E}_{p(f_T^{out})} \left[\log p(f_T^{out}) - \mathbb{E}_{p(f_S^{in})} [\log p(f_T^{out} | f_S^{in})] \right]. \end{aligned}$$

According to the definition of the marginal distribution, we have,

$$p(f_T^{out}) = \int_{\mathbb{R}^d} p(f_T^{out} | f_S^{in}) p(f_S^{in}) df_S^{in} = \mathbb{E}_{p(f_S^{in})} [p(f_T^{out} | f_S^{in})].$$

Since $\forall x > 0, x > \log x$, therefore, we have

$$\begin{aligned} \hat{I}(f_S^{in}, f_T^{out}) - I(f_S^{in}, f_T^{out}) &= \mathbb{E}_{p(f_T^{out})} \left[\log p(f_T^{out}) - \mathbb{E}_{p(f_S^{in})} [\log p(f_T^{out} | f_S^{in})] \right] \\ &= \mathbb{E}_{p(f_T^{out})} \left[\log \left(\mathbb{E}_{p(f_S^{in})} [p(f_T^{out} | f_S^{in})] \right) - \right. \\ &\quad \left. \mathbb{E}_{p(f_S^{in})} [\log p(f_T^{out} | f_S^{in})] \right]. \end{aligned}$$

Since $\log(\cdot)$ is a concave function and according to Jensen's inequality, we have

$$\begin{aligned} &\log \left(\mathbb{E}_{p(f_S^{in})} [p(f_T^{out} | f_S^{in})] \right) - \mathbb{E}_{p(f_S^{in})} [\log p(f_T^{out} | f_S^{in})] \\ &= \log \int_{\mathbb{R}^d} p(f_T^{out} | f_S^{in}) p(f_S^{in}) df_S^{in} - \int_{\mathbb{R}^d} \log [p(f_T^{out} | f_S^{in})] p(f_S^{in}) df_S^{in} \geq 0. \end{aligned}$$

Therefore, $\hat{I}(f_S^{in}, f_T^{out})$ is an upper bound of $I(f_S^{in}, f_T^{out})$. □

A.4 Proof for Theorem 2

Proof. For simplicity, we first give the following assumptions to prove the theorem.

Assumption 1. Assume that the samples $S = (x_1, \dots, x_m)$ and the labels $(c(x_1), \dots, c(x_m))$ are identically distributed according to the ID data distribution \mathcal{D}^m , which follows Gaussian mixture distribution.

Assumption 2. Assume that we only use the contrastive loss part in \mathcal{L}_{total} to train our model. In fact, the proof is similar to use all terms in \mathcal{L}_{total} .

Our task is to use the labeled sample S to learn a hypothesis $h_S \in \mathcal{H}$ that has a small generalization error with respect to concept c .

Define concept $c : \mathcal{X} \rightarrow \mathcal{Y}$ is a mapping from \mathcal{X} to \mathcal{Y} . A concept class \mathcal{C} is a set of concepts that we wish to learn.

The generalization error between the hypothesis h and the target concept $c \in \mathcal{C}$ underlying distribution \mathcal{D}^m can be written as

$$R(h) = \mathbb{P}_{x \sim \mathcal{D}^m} [h(x) \neq c(x)].$$

In the stochastic scenario case, the output label is a probabilistic function of the input. Thus, we use the following extension framework of PAC-learning to prove our theorem.

Definition 1. Let \mathcal{H} be a hypothesis set. \mathcal{A} is an agnostic PAC-learning algorithm if there exists a polynomial function $poly(\cdot, \cdot, \cdot, \cdot)$ such that for any $\varepsilon > 0, \delta > 0$, for all distributions \mathcal{D} over $\mathcal{X} \times \mathcal{Y}$, the following holds for any sample size $m > poly(1/\varepsilon, 1/\delta, n, size(c))$:

$$\mathbb{P}_{S \sim \mathcal{D}^m} [R(h_S) - \min_{h \in \mathcal{H}} R(h) \leq \varepsilon] \geq 1 - \delta.$$

If \mathcal{A} further runs in $poly(1/\varepsilon, 1/\delta, n, size(c))$, then it is said to be an efficient agnostic PAC-learning algorithm.

The advantage of using this definition is that the distribution \mathcal{D} can be arbitrary, which makes it well applied to any scenario.

Therefore, we denote $R(h_S)$ as the generalization error for using $I(f_S^{in}, f_T^{out})$, $R_{sup}(h_S)$ as the generalization error for using $I_{sup}(f_S^{in}, f_T^{out})$. Furthermore, the algorithm is agnostic PAC-learnable when using I and I_{sup} to train the model.

Then, when using I to train the model, \exists a polynomial function $poly(\cdot, \cdot, \cdot, \cdot)$ such that $\forall \varepsilon, \delta > 0$, for all distribution \mathcal{D} over $\mathcal{X} \times \mathcal{Y}$, then $\forall m \geq poly(1/\varepsilon, 1/\delta, size(c))$, we have

$$\mathbb{P}_{S \sim \mathcal{D}^m} [R(h_S) - \min_{h \in \mathcal{H}} R(h) \leq \varepsilon] \geq 1 - \delta. \quad (4)$$

Similarly, there exists a polynomial $poly_{sup}(\cdot, \cdot, \cdot, \cdot)$ such that for the above ε, δ and distribution \mathcal{D} , $\forall m \geq poly_{sup}(1/\varepsilon, 1/\delta, size(c))$, we have

$$\mathbb{P}_{S \sim \mathcal{D}^m} [R_{sup}(h_S) - \min_{h \in \mathcal{H}} R_{sup}(h) \leq \varepsilon] \geq 1 - \delta. \quad (5)$$

Therefore, let the polynomial function as

$$\sup \{poly(1/\varepsilon, 1/\delta, size(c)), poly_{sup}(1/\varepsilon, 1/\delta, size(c))\},$$

then both equation (4) and (5) satisfy and our theorem holds.

□

A.5 Theoretical Justification for Why OAML Work

Before discussing why OAML work for OOD detection performance enhancement, we give the following assumptions.

Assumption 3. *Assume that the ID data follows a mixture of Gaussian distribution with unequal prior.*

Specifically, the density function of ID data distribution P^{in} can be written as follows,

$$\begin{aligned} p^{in}(\mathbf{x}) &= \sum_{j=1}^k w_j p_{\mathcal{X}|\mathcal{Y}}^{in}(\mathbf{x}|y_j) \\ &= \frac{\sum_{i=1}^k w_i \exp(-\frac{1}{2}(\mathbf{x} - \boldsymbol{\mu}_i)^\top \Sigma^{-1}(\mathbf{x} - \boldsymbol{\mu}_i))}{\sqrt{(2\pi)^d |\Sigma|}}. \end{aligned}$$

where \mathbf{x} represents the image sample from input space \mathcal{X} , $\mathcal{Y} = \{y_i\}_{i=1}^k$ is the label space, $\boldsymbol{\mu}_i$ ($i = 1, \dots, k$, k is the number of class) is the mean of class $y_i \in \mathcal{Y}$, w_i is the weight of each class i , and $\Sigma = \sigma^2 \mathbf{I} \in \mathbb{R}^{d \times d}$ is the covariance matrix, σ is the standard deviation value, d is the dimension of the feature space.

Then, from the perspective of generalization error, we can show the following Proposition.

Proposition 1. *Denote \mathcal{H} as the hypothesis space on ID data. Let*

$$R(h) = \mathbb{E}_{\mathbf{x} \sim \mathcal{D}^{in}} \left[\sum_{i=1}^k \mathbb{I}_{[h(\mathbf{x})]_i \neq [f(\mathbf{x})]_i} \right]$$

as the generalization error of $h \in \mathcal{H}$ on ID data \mathcal{D}^{in} , where $h(x)$ is the predicted value and $f(x)$ is the target value, \mathbb{I} is the indicator function, k is the number of classes. For a score function S , denote the False Positive Rate as $FPR(S)$. Then $FPR(S)$ is bounded by $\inf_{h \in \mathcal{H}} R(h)$.

Proof. For fixed $i \in [1, k]$, $i \in \mathbb{Z}$, the class-conditioned test OOD distribution can be any distribution of the following distribution family:

$$\bigcup_{i=1}^k \{P^{ood}(\mathbf{x}^{ood}|y_i)\} = \bigcup_{i=1}^k \{\mathbf{x}^{ood} : \Pr[\|\mathbf{x}^{ood} - \boldsymbol{\mu}_i\|_2 \leq \tau] \leq \varepsilon_\tau\}, \quad (6)$$

where $\tau = \sigma\sqrt{d} + \sigma\gamma + \varepsilon\sqrt{d}$, $\gamma \in (0, \sqrt{d})$, is a parameter that indicates the margin between ID and OOD distributions, ε_τ and ε are arbitrary sufficiently small numbers.

Take $\varepsilon_\tau = \inf_{h \in \mathcal{H}} R(h)$, then we have

$$\begin{aligned}
FPR(S) &= \frac{1}{k} \sum_{i=1}^k \mathbb{E}_{\mathbf{x} \sim P^{ood}(\mathbf{x}^{ood}|y_i)} \mathbb{I}[\|\mathbf{x} - \boldsymbol{\mu}_i\|_2 \leq r] \\
&\leq \sup_{1 \leq i \leq k} \mathbb{E}_{\mathbf{x} \sim P^{ood}(\mathbf{x}^{ood}|y_i)} \mathbb{I}[\|\mathbf{x} - \boldsymbol{\mu}_i\|_2 \leq r] \\
&\leq \sup_{1 \leq i \leq k} \mathbb{E}_{\mathbf{x} \sim P^{ood}(\mathbf{x}^{ood}|y_i)} \mathbb{I}[\|\mathbf{x} - \boldsymbol{\mu}_i\|_2 - \sqrt{d}\varepsilon \leq \sigma\sqrt{d} + \sigma\gamma] \\
&= \sup_{1 \leq i \leq k} \Pr[\|\mathbf{x} - \boldsymbol{\mu}_i\|_2 \leq \tau] \\
&\leq \varepsilon_\tau = \inf_{h \in \mathcal{H}} R(h).
\end{aligned}$$

where $r = (1 + \gamma/4\sqrt{d})\hat{\sigma}$ and $\hat{\sigma}^2 = \frac{1}{n} \sum_{i=1}^n \|\mathbf{x}_i - \bar{\mathbf{x}}\|_2^2$.

□

The above proof implies that the better the model's generalization ability over ID data, the lower its corresponding FPR value will be, which indicates higher OOD detection performance.

A.6 Visualization of the Generated Outliers

In this subsection, we visualize the OOD features/images generated by Stable Diffusion taking CIFAR-100 [20] as ID data in Figure 7. The subplot (a) shows the ID sample before OOD sampling, (b) is the OOD feature decoded via Stable Diffusion [29], and (c) is the corresponding OOD sample generated at pixel-level.



Fig. 7: The visualization of the OOD feature output by Stable Diffusion on CIFAR-10 [20] dataset. The subplot (a) displays the original image sample, (b) denotes the OOD features in the middle layer in SD, and (c) is the feature decoded in pixel space.